

# UC Berkeley

## UC Berkeley Previously Published Works

### Title

Simultaneous single-nucleus RNA sequencing and single-nucleus ATAC sequencing of neuroblastoma cell lines.

### Permalink

<https://escholarship.org/uc/item/54w8c5sf>

### Journal

Scientific Data, 11(1)

### Authors

Guyer, Richard  
Mueller, Jessica  
Picard, Nicole  
[et al.](#)

### Publication Date

2024-11-07

### DOI

10.1038/s41597-024-04061-x

Peer reviewed



OPEN

DATA DESCRIPTOR

# Simultaneous single-nucleus RNA sequencing and single-nucleus ATAC sequencing of neuroblastoma cell lines

Richard A. Guyer<sup>1,2</sup>  , Jessica L. Mueller<sup>2</sup>, Nicole Picard<sup>2</sup> & Allan M. Goldstein<sup>2</sup> 

Neuroblastoma is the most common extracranial solid tumor in children, and a leading cause of childhood cancer deaths. All neuroblastomas arise from neural crest-derived sympathetic neuronal progenitors, but numerous mutations, the most common of which is MYCN amplification, give rise to these lesions. Epigenetic aberrations also play a role in oncogenesis and tumor progression. To better understand biologic diversity of neuroblastomas, we performed joint single-nucleus ATAC sequencing and single-nucleus RNA sequencing on six neuroblastoma cell lines, three of which are MYCN amplified. After standard filtering for high-quality nuclei, we obtained chromatin accessibility and transcript abundance data from 41,733 neuroblastoma tumor cells. Preliminary analysis reveals significant diversity in chromatin landscape and gene expression across neuroblastoma cell lines. This dataset is a valuable resource for studying the transcriptional and epigenetic mechanisms of this deadly childhood disease.

## Background & Summary

Neuroblastoma is the most common extracranial solid tumor in children, with an especially high incidence among children under age 4 years<sup>1</sup>. The disease is stratified into low-risk, intermediate-risk, and high-risk categories, based on clinical and biological features. High-risk disease is fatal in over 60% of cases<sup>2</sup>. MYCN amplification is the most common mutation in neuroblastoma, and the presence of MYCN amplification is sufficient to designate a tumor as high-risk<sup>3</sup>. However, over half of high-risk lesions lack this mutation<sup>4,5</sup>, indicating significant biological diversity between neuroblastoma cases. Due to the challenges of obtaining primary tumor samples, various neuroblastoma cell lines have been established from high-risk lesions and are widely used for studying tumor biology.

There are numerous publicly-available transcriptional and epigenetic datasets derived from neuroblastoma cell lines, but information regarding heterogeneity within cell lines is not captured by the bulk methods used to generate these data<sup>6–8</sup>. The advent of single-cell sequencing tools has permitted high-parameter profiling of transcript abundance and epigenetic features in many cancers<sup>9</sup>. Several studies have reported single-cell RNA sequencing on neuroblastoma tissue, and have demonstrated considerable transcriptional heterogeneity within tumors as well as between cases<sup>10–13</sup>. Single-cell multiomic tools have been developed that measure two or more features (such as transcript abundance and chromatin accessibility) simultaneously from individual cells<sup>14</sup>. To our knowledge, however, multiome technology has not yet been applied to neuroblastoma.

We undertook the present study to better understand transcriptional and epigenetic diversity of human neuroblastoma cell lines, both within and between samples. We utilized six widely-studied neuroblastoma cell lines, features of which are displayed in Table 1, including MYCN amplification status and whether each line is known to have adrenergic or mesenchymal transcriptional circuitry<sup>15,16</sup>. One of these lines, SH-SY5Y, is a subclone derivative of another, SK-N-SH. By jointly quantifying transcript abundance and chromatin accessibility in individual nuclei, we provide a resource for studying the complex regulation of tumor cell phenotype. We anticipate

<sup>1</sup>Division of Pediatric Surgery, Department of Surgery, Johns Hopkins University School of Medicine, Baltimore, MD, USA. <sup>2</sup>Department of Pediatric Surgery, Massachusetts General Hospital, Boston, MA, USA. ✉e-mail: [rguyer2@jh.edu](mailto:rguyer2@jh.edu); [agoldstein@mgb.org](mailto:agoldstein@mgb.org)

Cell Line	MYCN status	Mesenchymal vs Adrenergic	Cells retained for analysis
SH-SY5Y	Non-amplified	Adrenergic	5,480
SK-N-SH	Non-amplified	Mesenchymal	5,977
SK-N-AS	Non-amplified	Mesenchymal	7,459
SK-N-DZ	Amplified	Adrenergic	5,295
CHP134	Amplified	<i>not reported in literature</i> <sup>15,16</sup>	5,827
Be2c	Amplified	Adrenergic	11,695

**Table 1.** Characteristics of cell lines studied.

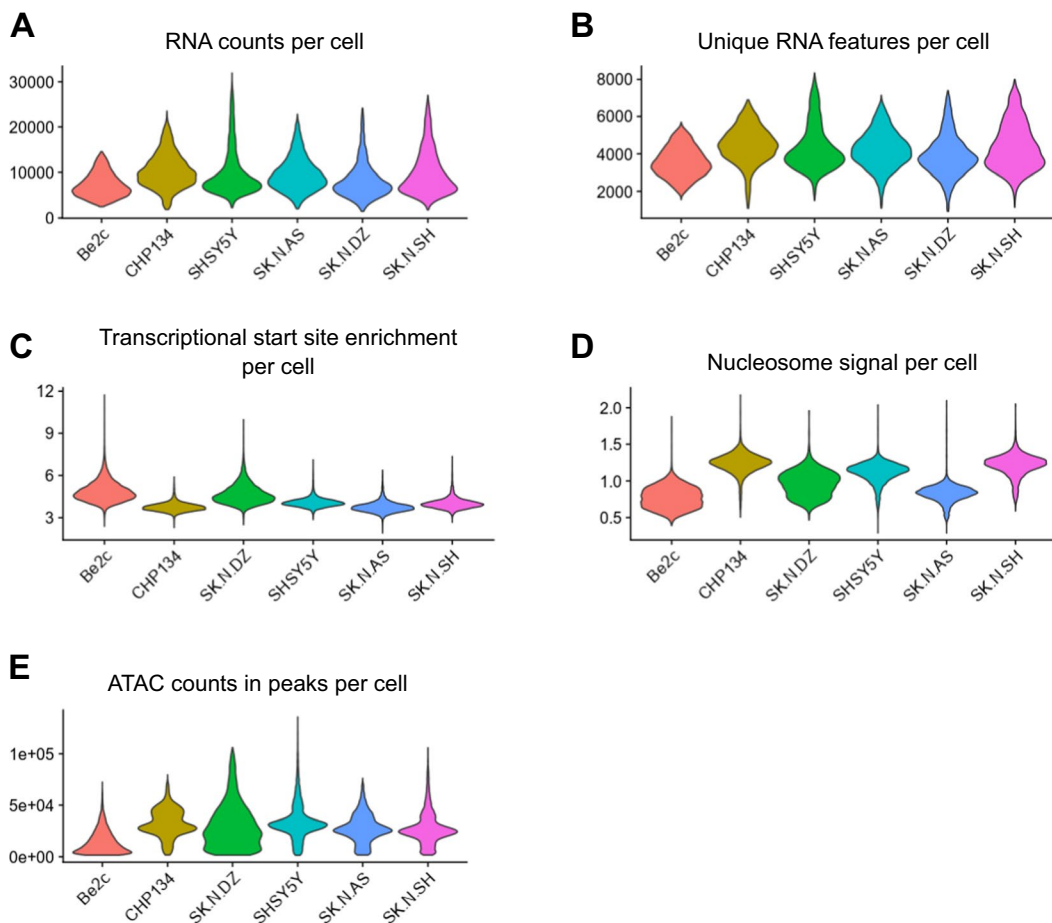


**Fig. 1** Quality control analysis of single-nucleus datasets. **(A)** Violin plot showing RNA counts in each cell in the snRNA-seq dataset, with the cell line indicated on the X-axis. **(B)** Violin plot showing unique RNA features identified in each cell in the snRNA-seq dataset, with the cell line indicated on the X-axis. **(C)** Violin plot showing transcriptional start site enrichment in each cell in the snATAC-seq dataset, with the cell lines indicated on the X-axis. **(D)** Violin plot showing nucleosome signal in each cell in the snATAC-seq dataset, with the cell lines indicated on the X-axis. **(E)** Violin plot showing ATAC counts in MACS2-identified peaks in each cell in the snATAC-seq dataset, with the cell lines indicated on the X-axis.

these data will be extremely useful for identifying the driver genes, transcriptional regulatory networks, and transcription factor-chromatin interactions underlying neuroblastoma cell states.

## Methods

**Cell lines and culture.** Cell lines used in this study were purchased from ATCC (Manassas, VA). All cell growth and preparation for sequencing was done at Massachusetts General Hospital. Cells were cultured under conditions recommended by ATCC. All cells were maintained in incubators at 37 °C and 5% CO<sub>2</sub>. Cells were passaged when they reached approximately 80% confluency. In all cases, cells were prepared for sequencing at a passage number less than 10.

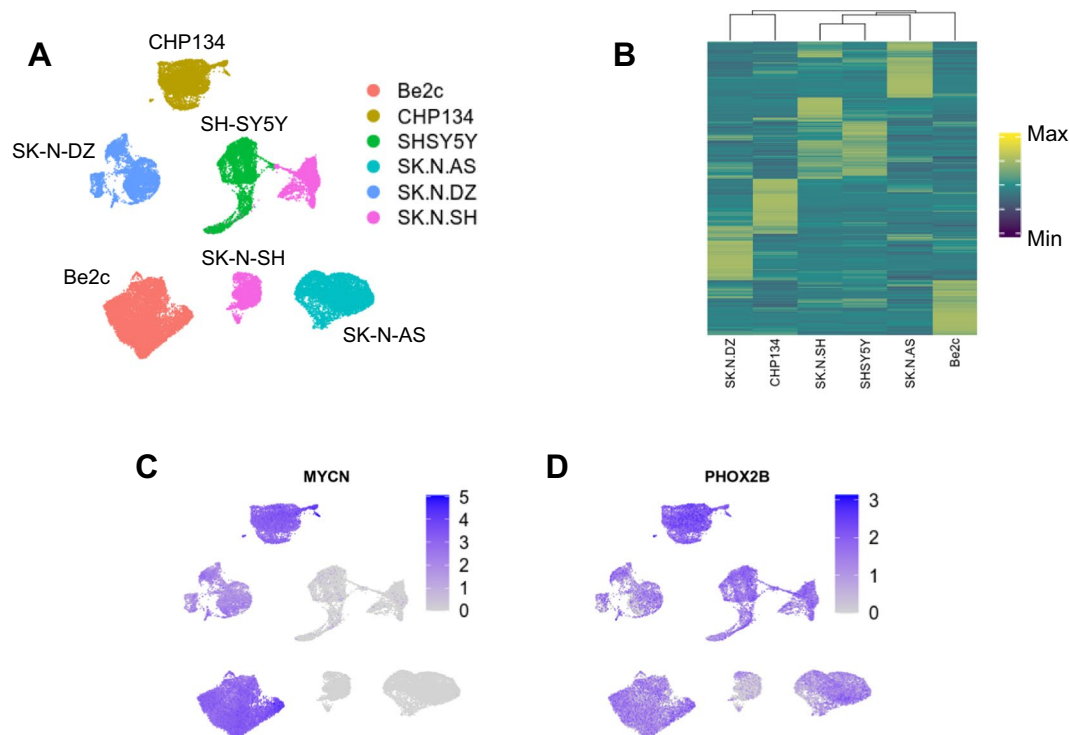


**Fig. 2** Basic analysis of snRNA-seq data. (A) UMAP projection showing cells from each cell line largely cluster together based on transcript abundance. (B) Heatmap showing mean expression in each cell line of the top 250 marker genes identified for each cell line. (C) Transcript abundance of *MYCN* within each cell, overlaid on the UMAP projection shown in (A). As anticipated, *MYCN*-amplified cell lines have markedly higher *MYCN* transcript levels. (D) Transcript abundance of *PHOX2B* within each cell, overlaid on the UMAP projection shown in (A). In contrast with *MYCN*, *PHOX2B* transcripts are abundant in all cell lines.

**Sample preparation.** Nuclei were isolated from individual cells using the 10X Genomics (Pleasanton, CA) Demonstrated Protocol CG000365: Nuclei Isolation for Single Cell Multiome ATAC + Gene Expression Sequencing. Briefly, cells were washed with cold PBS and trypsinized to a single-cell suspension. After pelleting at 300 rcf in a tabletop centrifuge in 15 mL conical tubes, cells were washed twice in 1 mL cold PBS supplemented with 0.04% BSA. Cells were then passed through a 40  $\mu$ m strainer and counted using a standard hemocytometer. A total of 1,000,000 cells were transferred to 2 mL microcentrifuge tubes. Cells were resuspended in 100 mL of ice-cold Lysis Buffer (10 mM Tris-HCl at pH 7.4, 10 mM NaCl, 3 mM MgCl<sub>2</sub>, 0.1% Tween-20, 0.1% NP-40, 0.01% digitonin, 1% BSA, 1 mM DTT, 1 U/mL RNase inhibitors, all in nuclease-free water) and incubated for 4 minutes on ice, followed by addition of 1 mL of Wash Buffer (10 mM Tris-HCl at pH 7.4, 10 mM NaCl, 3 mM MgCl<sub>2</sub>, 1% BSA, 0.1% Tween-20, 1 mM DTT, and 1 U/mL RNase inhibitors in nuclease-free water). Cells were centrifuged at 500 rcf for 5 minutes at 4 °C to repellet. A total of 3 washes in Wash Buffer were performed. Cells were then suspended in 1 mL of 1x Nuclei Buffer (provided at 20x concentration by 10X Genomics in Chromium Next GEM Single Cell Multiome ATAC Kit A, PN-1000280) supplemented with 1 mM DTT and 1 U/mL RNase inhibitors. GEM generation and cell barcoding were immediately performed using 10X Genomics Chromium Controller and 10X Genomics Next GEM Chip J. ATAC and gene expression library construction was performed per the 10X Genomics Next GEM Single Cell Multiome ATAC + Gene Expression User Guide, with reagents purchased from 10X Genomics. Sequencing was performed on the Illumina NovaSeq platform at the Harvard University Bauer Core facility.

**Data analysis.** ATAC and gene expression FASTQ output files were demultiplexed and mapped to the Genome Reference Consortium hg38 reference genome with Cell Ranger ARC (10X Genomics) software on the Harvard University Bauer Core's computing cluster. The resulting fragment files and count matrices were processed further using Signac version 1.1.0 and Seurat version 4.3.0.1, and implemented in R version 4.3.2 in the Rstudio computing environment version 2023.03.1 + 446. High-quality nuclei were selected based on the following criteria: ATAC counts > 2500 and < 1000000, RNA counts > 2000 and < 10000, nucleosome signal < 2, transcriptional start site enrichment > 1, and mitochondrial RNA < 5% of total transcripts. Table 1 shows the number of cells from each line retained after quality filtering. ATAC peak calling was performed using the Signac "CallPeaks" function and MACS2 version 2.2.7.1. The standard Seurat and Signac workflows were then used to analyze data. Marker peaks for each cell line with the ATAC data were identified using the Seurat "FindAllMarkers" function with default arguments, except for the following: only.pos = "TRUE", test.use = "LR", and latent.vars = "nCount\_ATAC". Similarly, marker genes for each cell line were identified with the same function, with the following adjustments to default arguments: only.pos = "TRUE", logfc.threshold = 0.5, and min.pct = 0.2.

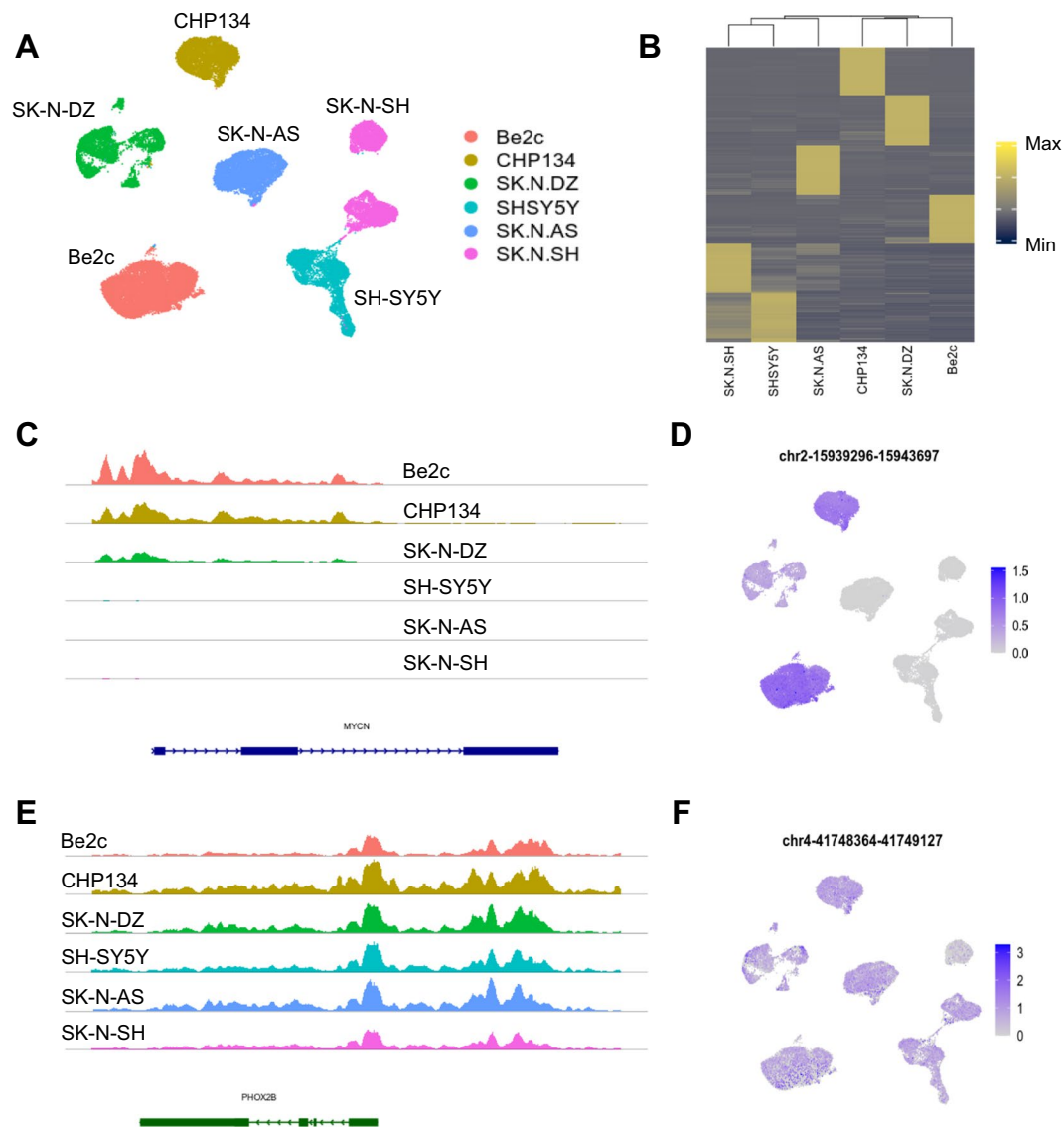


**Fig. 3** Basic analysis of snATAC-seq data. **(A)** UMAP projection showing cells from each cell line largely cluster together based on chromatin accessibility. **(B)** Heatmap showing mean expression in each cell line of the top 1000 marker peaks identified for each cell line. **(C,E)** Track plots showing ATAC counts in and around the *MYCN* and *PHOX2B* coding sequences in the indicated cell lines. **(D,F)** ATAC count abundance within each cell for the indicated MACS2 peaks, which lie within the *MYCN* **(D)** and *PHOX2B* **(F)** coding regions, overlaid on the UMAP projection shown in **(A)**.

### Data Records

Raw FASTQ files, count matrices in CSV format, and key Cell Ranger output files (filtered gene expression feature matrices and ATAC fragment files) have been uploaded to the NCBI Gene Expression Omnibus, with accession number GSE262189<sup>17</sup>. RDS files containing Seurat objects derived from analyzing each cell line as described here have been uploaded to Mendeley Data, with the following DOIs and corresponding URLs: 10.17632/wvzz6hbtg.2 (<https://data.mendeley.com/datasets/wvzz6hbtg/1>)<sup>18</sup>, <https://doi.org/10.17632/29g4826npf.1> (<https://data.mendeley.com/datasets/29g4826npf/1>)<sup>19</sup>, <https://doi.org/10.17632/9yc8d8bnss.1> (<https://data.mendeley.com/datasets/9yc8d8bnss/1>)<sup>20</sup>, <https://doi.org/10.17632/cp4d7t74vb.1> (<https://data.mendeley.com/datasets/cp4d7t74vb/1>)<sup>21</sup>.

### Technical Validation

We evaluated standard quality control metrics for snRNA-seq and snATAC-seq datasets. After filtering for high-quality nuclei, as described above, our dataset consisted of 41,733 nuclei. The gene expression data showed consistency of counts per nucleus and unique features per nucleus across the six cell lines studied (Fig. 1A,B). Similarly, ATAC data was consistent across cell lines with respect to transcriptional start site enrichment, nucleosome signal, and the number of counts in peaks (Fig. 1C–E).

We performed basic dimensional reduction, clustering, and analysis using transcriptional data. As expected, there was more variation between cell lines than within cell lines, as demonstrated on a UMAP projection

(Fig. 2A). A subset of SK-N-SH cells does appear closely related to SH-SY5Y cells (Fig. 2A), which may be expected since SH-SY5Y cells are a subclone of the SK-N-SH line. We identified the top 250 marker genes for each cell line, relative to all other cell lines. Hierarchical clustering based on scaled expression of these 250 genes shows that the non-*MYCN*-amplified cell lines (SHSY5Y, SK-N-SH, and SK-N-AS) were most similar to one another, with SK-N-SH and SH-SY5Y being most similar, while the *MYCN*-amplified cell lines (CHP134, Be2c, and SK-N-DZ) diverged from the non-amplified lines (Fig. 2B). Next, we assessed gene expression of two important neuroblastoma driver genes: *MYCN* and *PHOX2B*. As anticipated, our data show markedly higher expression of *MYCN* transcripts in the *MYCN*-amplified cell lines (Fig. 2C), while *PHOX2B* transcripts are more uniformly distributed across all six cell lines (Fig. 2D).

Similarly, we assessed the chromatin accessibility dataset in each cell line. Just as for gene expression data, we found that the greatest variability was between cell lines, as visualized on a UMAP projection (Fig. 3A). The top 1000 marker peaks for each cell line were identified and used to generate a heatmap (Fig. 3B). Hierarchical clustering of this data shows that the three non-*MYCN*-amplified lines cluster together and maintain open chromatin at similar genomic regions. Again, both the UMAP projection and hierarchical clustering of the heatmap suggest a close relationship between the SH-SY5Y and SK-N-SH lines (Fig. 3A,B). In contrast, *MYCN*-amplified lines show more divergence in their chromatin accessibility patterns. Due to *MYCN* amplification, we expect the CHP134, Be2c, and SK-N-DZ cell lines to have far more counts mapped to the *MYCN* locus than the non-amplified lines. A tracks plot of the *MYCN* gene shows these results (Fig. 3C). Similarly, counts within the ATAC peak found at chromosome 2, bases 15,939,296–15,943,697, which lies within the *MYCN* coding sequence, are seen exclusively in the *MYCN*-amplified lines (Fig. 3D). In contrast, there is a similar chromatin signal in both the coding sequence and upstream promoter region of *PHOX2B*, including at the peak at chromosome 4, bases 41,748,364–41,749,127 (Fig. 3E,F).

### Code availability

R scripts use for processing and analysis of this data are publicly available at a Mendeley Data repository with <https://doi.org/10.17632/s2fcfb8phh.1> (<https://data.mendeley.com/datasets/s2fcfb8phh/1>)<sup>22</sup>.

Received: 10 April 2024; Accepted: 1 November 2024;

Published online: 07 November 2024

### References

- Li, J., Thompson, T. D., Miller, J. W., Pollack, L. A. & Stewart, S. L. Cancer Incidence Among Children and Adolescents in the United States, 2001–2003. *Pediatrics* **121**, e1470–e1477 (2008).
- Newman, E. A. *et al.* Update on neuroblastoma. *Journal of Pediatric Surgery* **54**, 383–389 (2019).
- Cohn, S. L. *et al.* The International Neuroblastoma Risk Group (INRG) Classification System: An INRG Task Force Report. *JCO* **27**, 289–297 (2009).
- Lee, J. W. *et al.* Clinical significance of *MYCN* amplification in patients with high-risk neuroblastoma. *Pediatr Blood Cancer* **65**, e27257 (2018).
- Yanishkevski, D. *et al.* Impact of *MYCN* status on response of high-risk neuroblastoma to neoadjuvant chemotherapy. *Journal of Pediatric Surgery* **55**, 130–134 (2020).
- Guyer, R. A. *et al.* Differentiated neuroblastoma cells remain epigenetically poised for de-differentiation to an immature state. *Disease Models & Mechanisms* **16**, dmm049754 (2023).
- Upton, K. *et al.* Epigenomic profiling of neuroblastoma cell lines. *Sci Data* **7**, 116 (2020).
- Harenza, J. L. *et al.* Transcriptomic profiling of 39 commonly-used neuroblastoma cell lines. *Sci Data* **4**, 170033 (2017).
- Kashima, Y. *et al.* Single-cell sequencing techniques from individual to multiomics analyses. *Exp Mol Med* **52**, 1419–1427 (2020).
- Dong, R. *et al.* Single-Cell Characterization of Malignant Phenotypes and Developmental Trajectories of Adrenal Neuroblastoma. *Cancer Cell* **38**, 716–733.e6 (2020).
- Mercatelli, D. *et al.* Single-Cell Gene Network Analysis and Transcriptional Landscape of *MYCN*-Amplified Neuroblastoma Cell Lines. *Biomolecules* **11**, 177 (2021).
- Jansky, S. *et al.* Single-cell transcriptomic analyses provide insights into the developmental origins of neuroblastoma. *Nature Genetics* **53**, 683–693, <https://doi.org/10.1038/s41588-021-00806-1> (2021).
- Kildisiute, G. *et al.* Tumor to normal single-cell mRNA comparisons reveal a pan-neuroblastoma cancer cell. *Science Advances* **7**, eabd3311 (2021).
- Ma, S. *et al.* Chromatin Potential Identified by Shared Single-Cell Profiling of RNA and Chromatin. *Cell* **183**, 1103–1116.e20 (2020).
- Boeva, V. *et al.* Heterogeneity of neuroblastoma cell identity defined by transcriptional circuitries. *Nature Genetics* **49**, 1408–1413, <https://doi.org/10.1038/ng.3921> (2017).
- van Groningen, T. *et al.* Neuroblastoma is composed of two super-enhancer-associated differentiation states. *Nature Genetics* **49**, 1261–1266, <https://doi.org/10.1038/ng.3899> (2017).
- Guyer, R. A. & Goldstein, A. M. *GEO* <https://identifiers.org/geo/GSE262189> (2024).
- Guyer, R. A. & Goldstein, A. M. Seurat objects for multiome analysis of neuroblastoma cell lines - 1/4. *Mendeley Data V1* <https://doi.org/10.17632/wvzz6hbtg.1> (2024).
- Guyer, R. A. & Goldstein, A. M. Seurat objects for multiome analysis of neuroblastoma cell lines - 2/4. *Mendeley Data V1* <https://doi.org/10.17632/29g4826npf.1> (2024).
- Guyer, R. A. & Goldstein, A. M. Seurat objects for multiome analysis of neuroblastoma cell lines - 3/4. *Mendeley Data V1* <https://doi.org/10.17632/9yc8d8bnss.1> (2024).
- Guyer, R. A. & Goldstein, A. M. Seurat objects for multiome analysis of neuroblastoma cell lines - 4/4. *Mendeley Data V1* <https://doi.org/10.17632/cp4d7t74vb.1> (2024).
- Guyer, R. A. & Goldstein, A. M. Analysis of multiome sequencing data from neuroblastoma cell lines. *Mendeley Data V1* <https://doi.org/10.17632/s2fcfb8phh.1> (2024).

### Acknowledgements

This work was supported by NIDDK F32DK121440 to RAG, NIDDK F32DK131792 to JLM, NIDDK R01DK119210 to AMG, and by the Massachusetts General Hospital Department of Surgery Patricia K. Donahoe Resident Research Catalyst Award to RAG. The authors thank the staff at the Harvard University Bauer Core for their expertise and assistance.

### Author contributions

R.A.G. and A.M.G. conceived and designed this project. R.A.G., J.L.M. and N.B. performed cell culture, sample preparation, and library construction. R.A.G. did all data analysis and processing. R.A.G. wrote all code used for data analysis. Funding for the project was obtained by R.A.G. and A.M.G. R.A.G. drafted the manuscript and prepared figures. All authors participated in manuscript editing, and all authors have approved the version of the manuscript submitted for publication.

### Competing interests

The authors declare no competing interests.

### Additional information

**Correspondence** and requests for materials should be addressed to R.A.G. or A.M.G.

**Reprints and permissions information** is available at [www.nature.com/reprints](http://www.nature.com/reprints).

**Publisher's note** Springer Nature remains neutral with regard to jurisdictional claims in published maps and institutional affiliations.



**Open Access** This article is licensed under a Creative Commons Attribution-NonCommercial-NoDerivatives 4.0 International License, which permits any non-commercial use, sharing, distribution and reproduction in any medium or format, as long as you give appropriate credit to the original author(s) and the source, provide a link to the Creative Commons licence, and indicate if you modified the licensed material. You do not have permission under this licence to share adapted material derived from this article or parts of it. The images or other third party material in this article are included in the article's Creative Commons licence, unless indicated otherwise in a credit line to the material. If material is not included in the article's Creative Commons licence and your intended use is not permitted by statutory regulation or exceeds the permitted use, you will need to obtain permission directly from the copyright holder. To view a copy of this licence, visit <http://creativecommons.org/licenses/by-nc-nd/4.0/>.

© The Author(s) 2024